



Article

# Friction and Tribo-Chemical Behavior of SPD-Processed CNT-Reinforced Composites

Katherine Aristizabal <sup>1,\*</sup> , Alexandra Tayrac <sup>1</sup>, Andreas Katzensteiner <sup>2</sup>, Andrea Bachmaier <sup>2</sup> and Sebastian Suarez <sup>1,\*</sup>

<sup>1</sup> Chair of Functional Materials, Saarland University, Campus D3.3, 66123 Saarbrücken, Germany

<sup>2</sup> Erich Schmid Institute of Materials Science, Austrian Academy of Sciences, Jahnstrasse 12, 8700 Leoben, Austria

\* Correspondence: katherine.aristizabal@uni-saarland.de (K.A.); s.suarez@mx.uni-saarland.de (S.S.)

Received: 10 July 2019; Accepted: 27 August 2019; Published: 30 August 2019



**Abstract:** Nickel (Ni) and carbon nanotube (CNT)-reinforced Ni-matrix composites were manufactured by solid state processing and severely deformed by high-pressure torsion (HPT). Micro-tribological testing was performed by reciprocating sliding and the frictional behavior was investigated. Tribo-chemical and microstructural changes were investigated using energy dispersive X-ray spectroscopy (EDS), scanning electron microscopy (SEM) and focused ion beam (FIB). The CNT lubricity was hindered due to the continuous formation of a stable oxide layer promoted by a large grain boundary area and by irreversible damage introduced to the reinforcement during HPT, which controlled the frictional behavior of the studied samples. The presence of CNT reduced, to some extent, the tribo-oxidation activity on the contact zone and reduced the wear by significant hardening and stabilization of the microstructure.

**Keywords:** carbon nanotubes; metal matrix composites; severe plastic deformation; reciprocating sliding

## 1. Introduction

In a tribological system, where two bodies are moving relative to each other with a certain speed under the application of a normal force ( $F_N$ ) and along a certain distance with certain environmental conditions (e.g., temperature and humidity), there are other aspects, such as the surface finish [1–4] and the microstructure [5–7], that affect the wear, the friction and even the tribo-oxidation on the contact zone. Furthermore, it has been shown that intermittent tribological loading induces plastic deformation in a layer beneath the wear track in the tribologically transformed zone (TTZ) [8], which could result in grain refinement (in initially coarse-grained materials) [4,9] or grain coarsening (in initially nanocrystalline materials) [4,6,7,10,11].

Tribological testing on ultrafine-grained (UFG) and nanocrystalline (NC) materials obtained by severe plastic deformation (SPD) can lead to interesting results, due to the different phenomena that can occur. For instance, despite the increase in hardness due to a finer microstructure that can lead to a decrease in the coefficient of friction (COF) and a decrease in the wear rate, corrosion and oxide formation can be promoted by the high amount of grain boundaries affecting both friction and wear. Accordingly, even though there are studies showing improved wear resistance in materials processed by equal-channel angular pressing (ECAP), high pressure torsion (HPT) and accumulative roll-bonding (ARB), there are studies showing reduced wear resistance and others showing that the processing routes had little influence on the wear behavior [12]. On the one hand, the factors improving the wear resistance in SPD-processed materials are the smaller grain sizes and the higher hardness and strength. On the other hand, factors such as the decreased ductility, the low strain hardening capability, the higher oxidation rate, the non-equilibrium and unstable grain boundaries, the strain-induced grain coalescence

and the strain incompatibility between surface and bulk materials are responsible for the reduction in wear resistance. For further information refer to [12] and the references therein.

Strategies have been proposed to improve the wear resistance in SPD-processed materials, such as heat treatments after processing, the use of hard coatings such as TiO<sub>2</sub>, TiN and diamond-like carbon, and the introduction of ceramic reinforcements such as SiC [13] and Al<sub>2</sub>O<sub>3</sub> [14]. Furthermore, carbon nanotubes (CNT) have proved to be suitable for their use as solid lubricants and have been used in metal matrix composites (MMC) [15–17]. Providing there is a weak bond between the CNT and the metal and the CNT are uniformly distributed, CNT will continuously move to the tribological contact to roll and slide and even form a lubricating carbon film by degrading the CNT, thus improving both the wear and the COF (see [18] and the references therein). Furthermore, CNT have also been used for the production of lubricating coatings. Reinert et al. [19] studied and compared the tribo-mechanisms of CNT in CNT/Ni matrix composites and CNT-coated bulk Ni; they found that the reduction in COF in the coating lasts as long as there are CNT at the contact zone. After removal, the COF increased, whereas in the composite the COF reduction is pronounced up to 20,000 cycles due to a continuous supply of CNT to the contact zone. Nevertheless, CNT coatings produced on laser-patterned surfaces showed a long-lasting solid lubrication, due to CNT entrapping inside the laser textures serving as lubricant reservoirs [20].

Several studies have been performed regarding the microstructural changes during HPT of CNT/Ni [21–25]. In this work, micro-tribological testing was performed on CNT/Ni matrix composites processed by SPD by means of HPT, a technique in which a cylindrical sample is pressed under high hydrostatic pressure (in this case 4 GPa) while the upper anvil is kept static and the lower anvil is rotated to obtain the desired equivalent strain. The equivalent strain ( $\varepsilon_{vM}$ ) increases with the radius according to:  $\varepsilon_{vM} = 2\pi \cdot T \cdot r / (t \cdot \sqrt{3})$ , where  $T$  is the number of turns,  $t$  is the sample thickness and  $r$  is the distance from the center of the sample [26]. Furthermore, the wear tracks were analyzed by means of scanning electron microscopy (SEM) and energy dispersive X-ray spectroscopy (EDS) in order to study the tribo-chemistry. Finally, the subsurface was studied by means of focused ion beam (FIB) in order to assess possible microstructural changes under the wear scar.

## 2. Materials and Methods

For the fabrication of the samples, multi-walled CNT (chemical vapor deposition –CVD-grown, Graphene Supermarket, Ronkonkoma, NY, USA, density 1.84 g/cm<sup>3</sup>) were mixed in different concentrations (0.5, 1 and 2 wt.%) with dendritic Ni powder (Alfa Aesar, Kandel, Germany, mesh –325) via colloidal mixing [27]. The powder mixtures were then cold pressed (990 MPa) in cylindrical pellets and sintered under vacuum ( $2 \times 10^{-6}$  mbar, 900 °C for 3 h). The cold pressed sintered (CPS) composites and Ni samples of 8 mm diameter and 1 mm thickness were plastically deformed by HPT at room temperature using 1, 10 and 20 T.

The samples were then polished until mirror finish,  $R_q = (3.9 \pm 0.9) \mu\text{m}$  (with OP-S colloidal silica, Struers, Willich, Germany), and tested using a ball-on-disk tribometer under a linear reciprocating motion using an Al<sub>2</sub>O<sub>3</sub> ball (3 mm diameter) as a counter body. Table 1 shows the parameters used for the tribological tests.

**Table 1.** Parameters of the tribological experiments.

Parameter	Unit	Value
Temperature	°C	25
Relative humidity	%	3.8
Load $F_N$	N	0.1
Sliding velocity $v$	mm/s	1
Stroke length	Mm	0.6

The samples were tested three times at 3 mm from the center (see Figure 1) and the results were averaged. Vickers micro hardness ( $HV_{0.3}$ ) measurements were performed at 3 mm from the samples' centers using an indenter Struers DuraScan 50/70/80 and 15 s of dwell time. Table 2 shows the corresponding average hardness results for the studied samples. Moreover, electron micrographs, FIB cross-sections and EDS analyses were performed on a Helios NanoLab™ 600 dual beam field emission microscope (FEI Company).

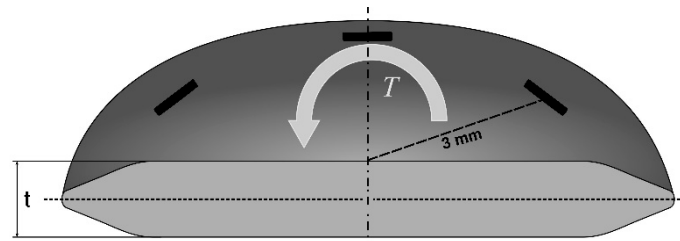


**Figure 1.** Schematic showing test positions.  $T$  indicates the direction of torsional rotation and  $t$  is the sample thickness.

**Table 2.** Hardness measured at 3 mm from the samples' centers with increasing equivalent strains.

Sample	Tested Equivalent Strain	Hardness/GPa
Ni_1T	14.51 ± 0.75	4.56 ± 0.09
Ni_10T	146.47 ± 4.54	4.78 ± 0.04
Ni_20T	310.67 ± 8.68	4.85 ± 0.10
0.5_1T	15.1 ± 0.65	3.92 ± 0.02
0.5_10T	134.94 ± 8.18	5.56 ± 0.05
0.5_20T	282.44 ± 25.89	6.44 ± 0.14
1_1T	15.76 ± 0.73	3.63 ± 0.02
1_10T	135.71 ± 3.48	6.33 ± 0.03
1_20T	281.86 ± 0	7.58 ± 0.41
2_1T	14.73 ± 1.09	3.58 ± 0.08
2_10T	149.57 ± 2.59	7.62 ± 0.03
2_20T	298.74 ± 14.23	8.01 ± 0.06

### 3. Results and Discussion

#### 3.1. Friction Analysis

Figure 2 shows the evolution of the COF for the tested samples and the corresponding run-in behavior. Considering the dispersion of results, no significant differences in COF for different concentrations of CNT and deformation states are noticeable (Figure 2a–c). In all cases, the steady state COF value oscillates around 0.3. The same effect has already been reported for SPD-processed Ti [28] where, despite testing two different initial microstructures (ultrafine and coarse-grained), the steady state COF was the same for a wide range of experimental loads.

The main differences are observed during the run-in stage (Figure 2d–f). In all cases, the pure Ni samples show a high initial COF value (between 0.55 and 0.6) that stabilizes after 20–30 cycles. The development of the COF curves for these samples indicates a significant plastic deformation at the beginning, subsequently achieving the steady state after reaching conformality. The CNT-containing sample shows a delayed stabilization, with indications of lower plastic deformation showing a steady state behavior first after 30–40 sliding cycles. The shape of these run-in curves is common in non-lubricated metals, where the COF increases temporarily due to the initial surface roughness and decreases after achieving surface conformality and smoothing [29].

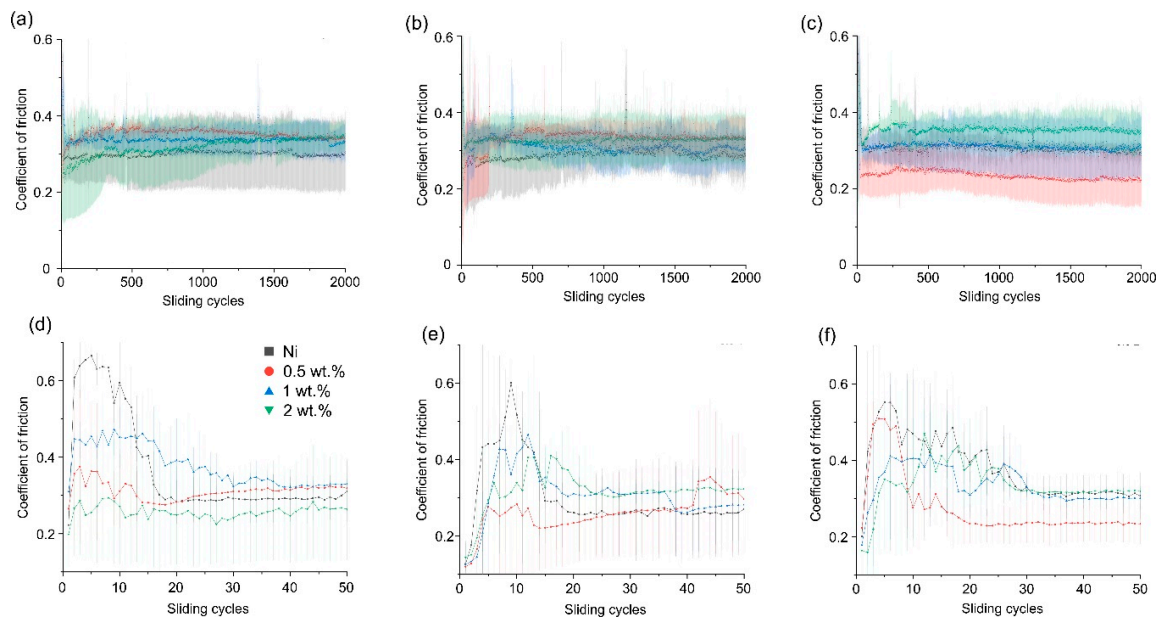


**Figure 2.** Evolution of the coefficient of friction (COF) versus the sliding cycles for: (a) 1 turn; (b) 10 turns; (c) 20 turns. Run-in behavior of the COF versus the sliding cycles for: (d) 1 turn; (e) 10 turns; (f) 20 turns.

The drop-in COF also takes place due to hardening of the near-surface regions due to shear stresses [29,30]. Furthermore, this slight increase in the COF and subsequent reduction can be attributed to the formation and release of debris (third body particles) into the contact, resulting from the continuous formation and breaking of a thin oxide layer reaching a dynamic balance in the steady state.

### 3.2. Wear Track Morphology and Tribo-Chemical Mechanisms

Further analysis of the results focuses on the samples subjected to the highest deformation (20 T). Figure 3 displays electron micrographs of the wear tracks. A first qualitative assessment suggests that the scar width is smaller in the composites. This can be attributed to a significantly harder surface in the composites, resulting in a smaller penetration depth of the counter body, which can be confirmed from the wear track profiles shown in Figure 4. Additionally, the characterization of the contact surface of the balls, shown in Figure 5, confirms that the wear activity of the counterpart was mild.

The pure metal sample shows regions of severe wear, indicated by the presence of laminated debris with partial detachment from the surface. This is extensively found within the affected zone and might be related to local thermal effects [31]. Furthermore, the tribologically affected surface shows significant continuity throughout the wear scar. The composite reinforced with 2 wt.% CNT presents evidence of mild wear associated with the development of a discontinuous tribolayer with almost no spallation and some scratch marks, which is typical of an abrasive mechanism [32]. The remaining sample (0.5 wt.% CNT) presents mild wear as well, but with evidence of both previously described cases. Certain regions show signs of galling, typical of a mild adhesive wear mechanism [32], whereas spallation and delamination of the tribolayer is noticed as well.

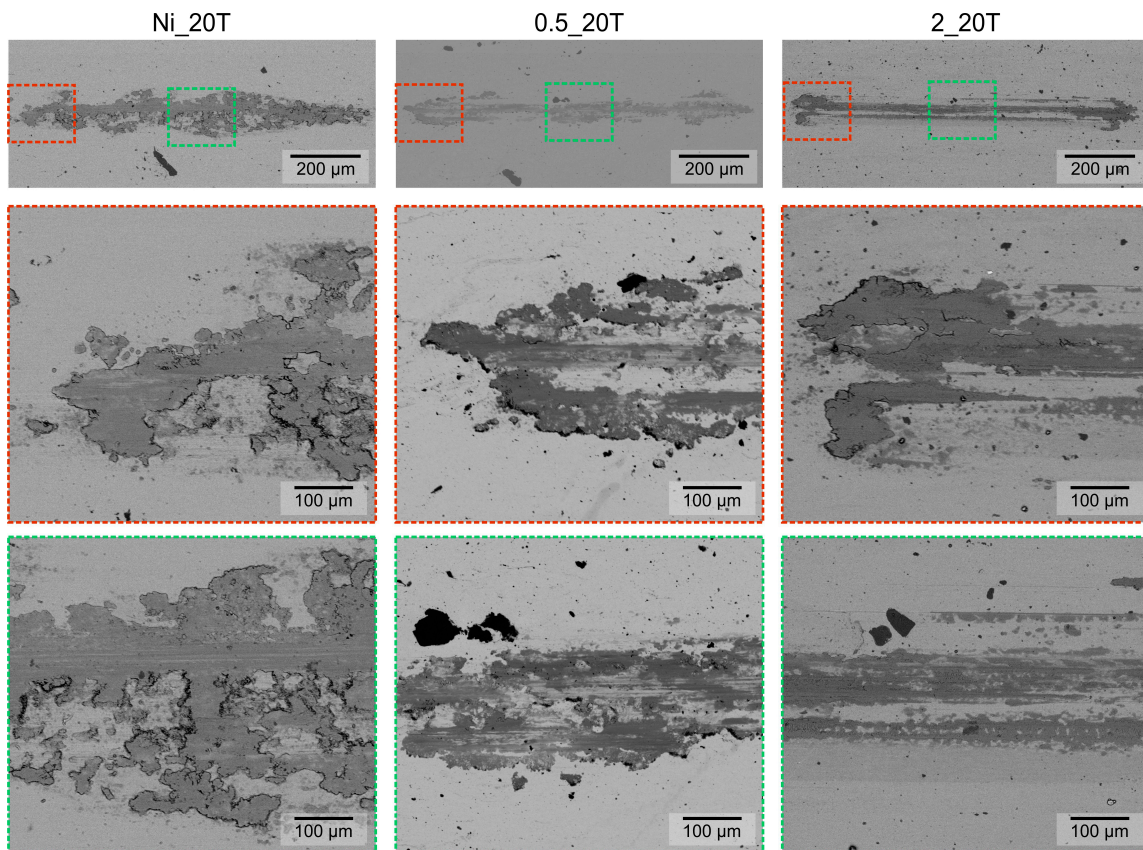


Figure 3. Electron micrographs on the wear scars.

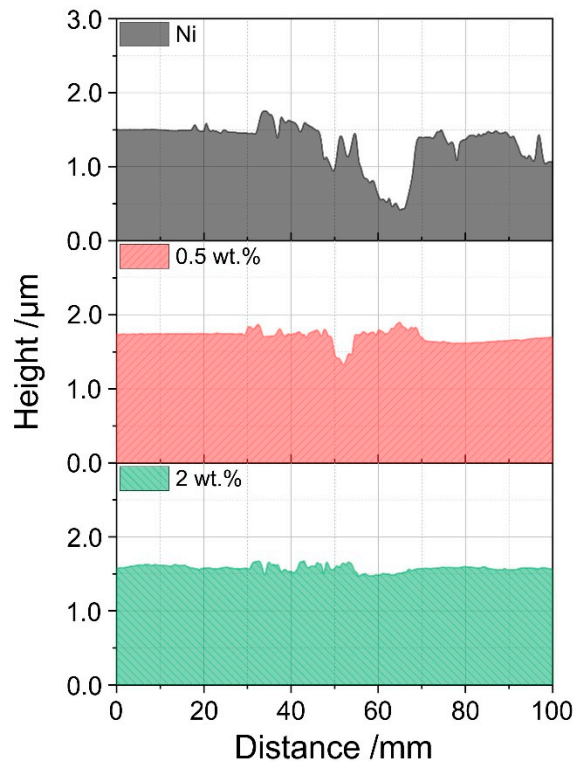
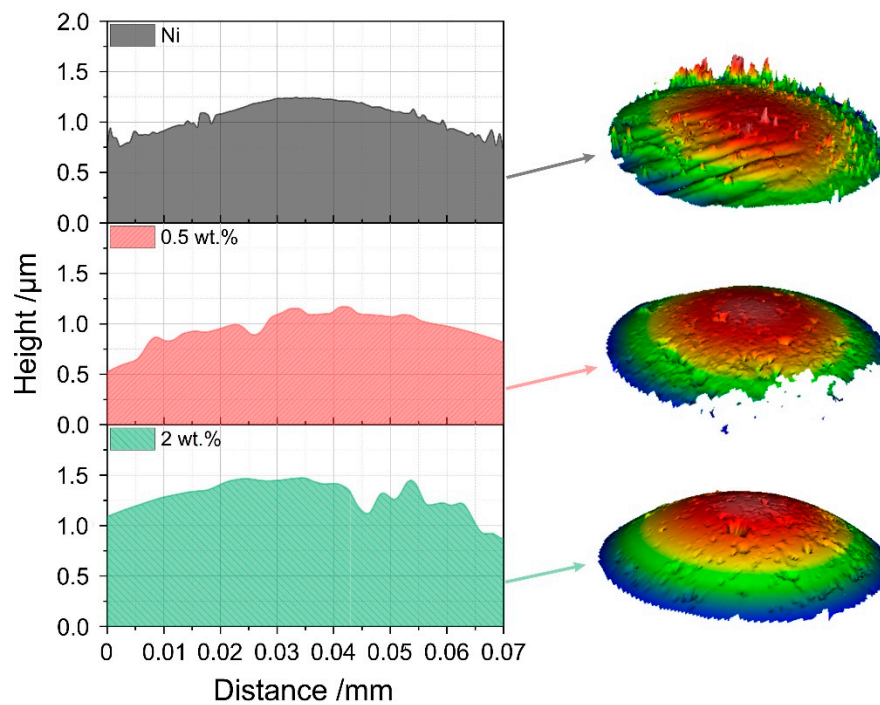
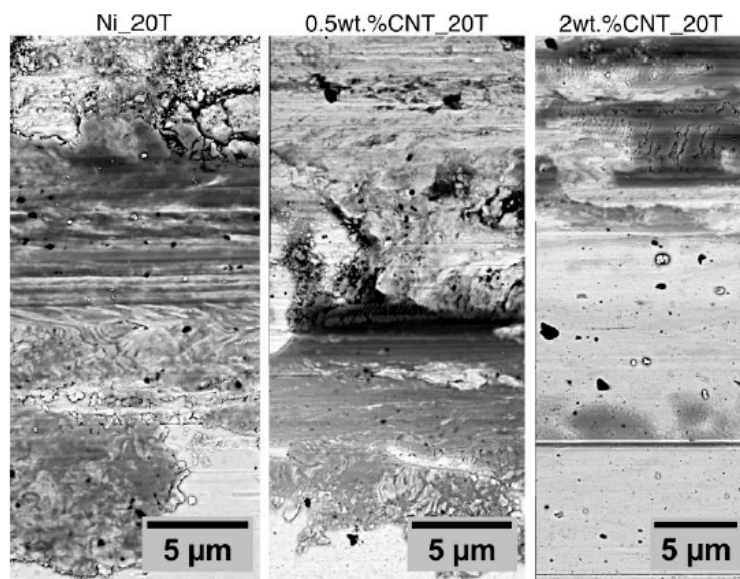


Figure 4. Wear track profiles for the samples deformed at 20 T obtained from the topographical characterization by means of confocal laser scanning microscopy.



**Figure 5.** Topographical profile and 3D map of the worn surface of the test counterparts acquired by white light interferometry.

Further morphological characteristics can be observed in detail in Figure 6, obtained with higher magnification from the edge of the central region of the tracks (in the sliding direction, where the maximum sliding velocity is obtained). These regions present indications of ploughing (for the pure metal and the 0.5 wt.% sample) and some wedge formation, which are characteristic of abrasive wear.



**Figure 6.** Detailed view of the wear scar edges at the center of the sliding track.

Nevertheless, adhesion and delamination of the oxide layer formed during sliding also occurred along with some intermixing with the metallic matrix. Such intermixing is less pronounced in the harder sample, which has grooves in the sliding direction, likely as a consequence of a reduced ductility [25] complicating the mechanical mixing process.

These observations were further expanded by performing a chemical analysis of the tribolayer to acquire oxygen distribution maps of the wear scar (Figure 7). In all cases, wear debris ejected from the tribological contact is observed (seen as small oxide particles outside the wear scar). The oxide layer appeared to be more pronounced in the case of pure Ni, which suggests that oxidation is reduced in the CNT-containing samples, at least from the observation of the total affected area. This observation is in agreement with the previously identified wear mechanisms [33]. The CNT brought into contact act as oxygen diffusion barriers, slowing the oxidation of the substrate. This is related to carbon being more prone to reactions with oxygen and its oxide being more stable than that of Ni.

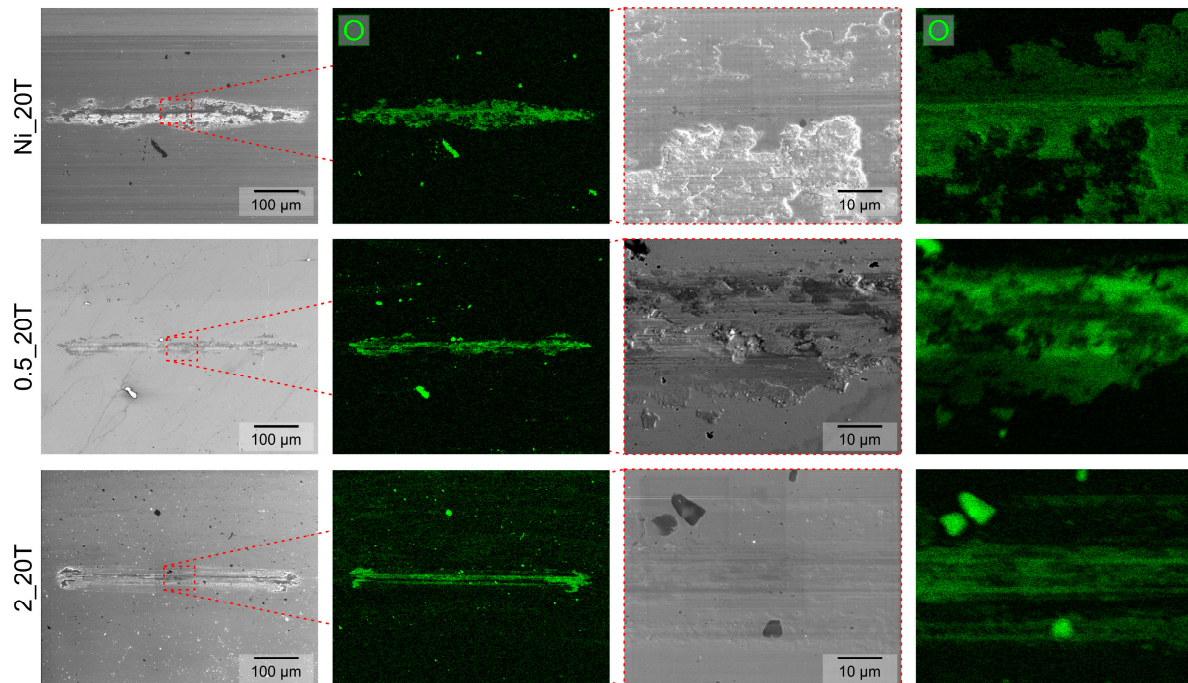


**Figure 7.** Oxygen distribution maps obtained by energy dispersive X-ray spectroscopy (EDS) from the wear tracks.

The lubrication mechanism of CNT in coarse-grained CNT/Ni matrix composites consists of the CNT being continuously provided to the contact zone, where a mixture between a rolling motion of the multiwall CNT on the surface and particle degradation occurs, including the formation of nanocrystalline graphitic layers [4]. For systems tested under the same experimental conditions, the lubricity of CNT is evidenced by a steady state COF of approximately 0.1, which is considerably below the COF obtained for the HPT-deformed systems. From the discussed results, the ultrafine-grained microstructures increase the oxidation activity of the surface due to a large grain boundary area. Moreover, even though the CNT distribution is significantly improved and the size of the agglomerates is significantly smaller in the deformed samples in comparison to the non-deformed samples [22], irreversible damage to the CNT is introduced by HPT [34] which renders them more susceptible to complete degradation and/or oxygen bonding. According to this, the CNT's ability to act as solid lubricants in the studied composites is strongly hindered. From these results, it can be concluded that in CNT/Ni matrix composites processed by HPT, the microstructure characteristics have a more significant effect on the steady state COF during sliding contact than the presence of CNT, which only slightly decrease the oxidation of the contact zone.

### 3.3. Microstructure under the Wear Scar

The analysis of the sub-superficial microstructural state was carried out on the same sample set by performing cross-sections in the middle of the wear scar (Figure 8). No significant microstructural

gradients beneath the surface are observed in any case, as opposed to what is expected when analyzing initially coarse-grained metals under dry sliding. This can be traced back to the fact that, for the TTZ to be developed, plastic deformation must occur beneath the worn surface due to the application of cyclic shear stresses. In the case of Ni (Figure 8a,b), the deformed sample (20 T of HPT) already achieved the microstructural steady state, as previously discussed [34]. Therefore, it is expected that no further microstructural changes or strain hardening would take place during strain accumulation.

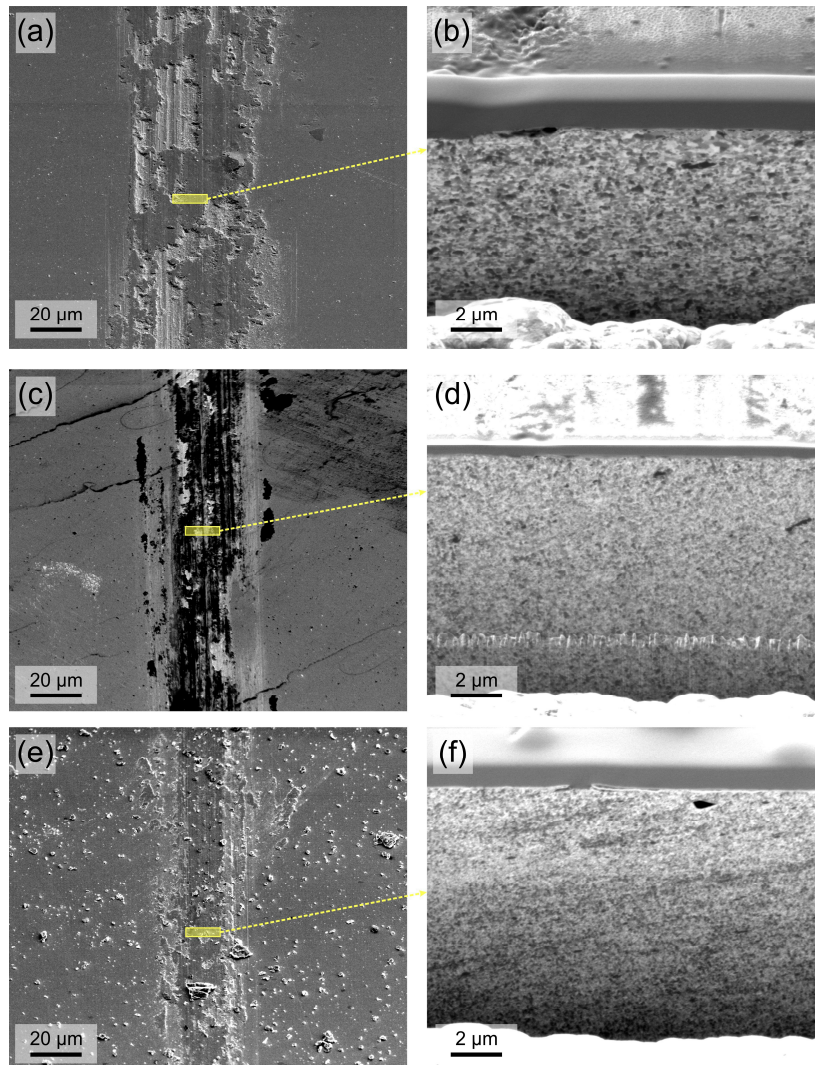


**Figure 8.** Cross-sections in the center of the wear scars in: (a,b) nickel; (c,d) 0.5 wt.% carbon nanotubes (CNT); (e,f) 2 wt.% CNT processed by high-pressure torsion (HPT) with 20 T.

In the case of the composites, even though the composites do not resemble the steady state hardness (as revealed in Table 2 by the continuously increasing hardness with higher accumulated equivalent strains), a significant reduction in grain size and a high density of defects [24] might be the defining factors. The maximum CNT distribution homogeneity was indeed achieved [22], which vouches for the proper microstructural stabilization, rendering the composites significantly harder and stable against possible microstructural changes induced during the tribological experiment.

To summarize, friction behavior is dominated by the quick formation of a tribologically induced oxide layer, which hinders the lubricity of the CNT. Wear, on the other hand, is reduced in the composites (when compared to the pure metal), resulting from a harder surface. Additionally, the presence of CNT aids in the stabilization of the microstructure during sliding, hence limiting the metal–oxide intermixing.

#### 4. Conclusions

In this paper, Ni and CNT/Ni composites with different CNT contents were processed by HPT with increasing equivalent strains. The resulting ultrafine-grained materials were tested by reciprocating sliding. The frictional, tribo-chemical and microstructural changes were investigated after 2000 sliding cycles. CNT structural defects, stemming from HPT processing and tribological contact, deterred their lubricity. The formation of a stable oxide layer also took place. As a result, the steady state COF stabilized around the same value ( $\mu_{\text{steady}} \approx 0.3$ ) for all the tested samples. No significant microstructural changes beneath the wear track were observed as a result of very hard surfaces, especially in the composites in which wear was reduced in comparison to Ni.

**Author Contributions:** S.S. and A.B. initiated the concepts and designed the experiments. K.A. and A.K. manufactured and processed the samples. K.A. and A.T. carried out the experiments. K.A. and S.S. characterized the samples, analyzed the data and wrote the manuscript. All authors reviewed and commented on the manuscript.

**Funding:** This research was funded by the Deutsche Forschungsgemeinschaft (DFG), grant number SU911/1-1 and the Fonds zur Förderung der wissenschaftlichen Forschung (FWF), grant number I2294-N36.

**Acknowledgments:** K.A. wishes to thank the German Academic Exchange Service (DAAD) (91567148) for their financial support. S.S. and K.A. gratefully acknowledge the financial support of DFG (Grant: SU911/1-1). A.B. and A.K. gratefully acknowledge the financial support of the Austrian Science Fund (FWF): I2294-N36.

**Conflicts of Interest:** The authors declare no conflict of interest. The funders had no role in the design of the study; in the collection, analyses, or interpretation of data; in the writing of the manuscript, or in the decision to publish the results.

#### References

1. Sedlaček, M.; Podgornik, B.; Vižintin, J. Influence of surface preparation on roughness parameters, friction and wear. *Wear* **2009**, *266*, 482–487. [[CrossRef](#)]
2. Meine, K.; Schneider, T.; Spaltmann, D.; Santner, E. The influence of roughness on friction Part I: The influence of a single step. *Wear* **2002**, *253*, 725–732. [[CrossRef](#)]
3. Meine, K.; Schneider, T.; Spaltmann, D.; Santner, E. The influence of roughness on friction: Part II. The influence of multiple steps. *Wear* **2002**, *253*, 733–738. [[CrossRef](#)]
4. Reinert, L.; Schütz, S.; Suárez, S.; Mücklich, F. Influence of surface roughness on the lubrication effect of carbon nanoparticle-coated steel surfaces. *Tribol. Lett.* **2018**, *66*, 45. [[CrossRef](#)]
5. Mishra, R.; Basu, B.; Balasubramaniam, R. Effect of grain size on the tribological behavior of nanocrystalline nickel. *Mater. Sci. Eng. A* **2004**, *373*, 370–373. [[CrossRef](#)]
6. Argibay, N.; Chandross, M.; Cheng, S.; Michael, J.R. Linking microstructural evolution and macro-scale friction behavior in metals. *J. Mater. Sci.* **2017**, *52*, 2780–2799.
7. Grützmacher, P.G.; Rammacher, S.; Rathmann, D.; Motz, C.; Mücklich, F.; Suarez, S. Interplay between microstructural evolution and tribo-chemistry during dry sliding of metals. *Friction* **2019**. [[CrossRef](#)]
8. Hutchings, I. *Tribology: Friction and Wear of Engineering Materials*, 2nd ed.; Elsevier: Oxford, UK, 2017.
9. Rigney, D.A.; Fu, X.Y.; Hammerberg, J.E.; Holian, B.L.; Falk, M.L. Examples of structural evolution during sliding and shear of ductile materials. *Scr. Mater.* **2003**, *49*, 977–983. [[CrossRef](#)]
10. Prasad, S.V.; Battaile, C.C.; Kotula, P.G. Friction transitions in nanocrystalline nickel. *Scr. Mater.* **2011**, *64*, 729–732. [[CrossRef](#)]
11. Wasekar, N.P.; Haridoss, P.; Seshadri, S.K.; Sundararajan, G. Sliding wear behavior of nanocrystalline nickel coatings: Influence of grain size. *Wear* **2012**, *296*, 536–546. [[CrossRef](#)]
12. Gao, N.; Wang, C.T.; Wood, R.J.K.; Langdon, T.G. Tribological properties of ultrafine-grained materials processed by severe plastic deformation. *J. Mater. Sci.* **2012**, *47*, 4779–4797. [[CrossRef](#)]
13. Darmiani, E.; Danaee, I.; Golozar, M.A.; Toroghinejad, M.R.; Ashrafi, A.; Ahmadi, A. Reciprocating wear resistance of Al-SiC nano-composite fabricated by accumulative roll bonding process. *Mater. Des.* **2013**, *50*, 497–502. [[CrossRef](#)]
14. Edalati, K.; Ashida, M.; Horita, Z.; Matsui, T.; Kato, H. Wear resistance and tribological features of pure aluminum and Al-Al<sub>2</sub>O<sub>3</sub> composites consolidated by high-pressure torsion. *Wear* **2014**, *310*, 83–89. [[CrossRef](#)]

15. Rajkumar, K.; Aravindan, S. Tribological studies on microwave sintered copper-carbon nanotube composites. *Wear* **2011**, *270*, 613–621. [[CrossRef](#)]
16. Bastwros, M.M.H.; Esawi, A.M.K.; Wifi, A. Friction and wear behavior of Al-CNT composites. *Wear* **2013**, *307*, 164–173. [[CrossRef](#)]
17. Abdullahi, U.; Maleque, M.A.; Nirmal, U. Wear mechanisms map of CNT-Al nano-composite. *Procedia Eng.* **2013**, *68*, 736–742. [[CrossRef](#)]
18. Dorri Moghadam, A.; Omrani, E.; Menezes, P.L.; Rohatgi, P.K. Mechanical and tribological properties of self-lubricating metal matrix nanocomposites reinforced by carbon nanotubes (CNTs) and graphene—A review. *Compos. Part B Eng.* **2015**, *77*, 402–420. [[CrossRef](#)]
19. Reinert, L.; Suárez, S.; Rosenkranz, A. Tribo-Mechanisms of Carbon Nanotubes: Friction and Wear Behavior of CNT-Reinforced Nickel Matrix Composites and CNT-Coated Bulk Nickel. *Lubricants* **2016**, *4*, 11. [[CrossRef](#)]
20. Reinert, L.; Lasserre, F.; Gachot, C.; Grützmacher, P.; Maclucas, T.; Souza, N.; Mücklich, F.; Suarez, S. Long-lasting solid lubrication by CNT-coated patterned surfaces. *Sci. Rep.* **2017**, *7*, 42873. [[CrossRef](#)] [[PubMed](#)]
21. Aristizabal, K.; Suárez, S.; Katzensteiner, A.; Bachmaier, A.; Mücklich, F. Evolution of the microstructure in carbon nanotube reinforced Nickel matrix composites processed by high-pressure torsion. In Proceedings of the IOP Conference Series: Materials Science and Engineering, Bristol, UK, 2017; Volume 258, No. 1, p. 012008.
22. Aristizabal, K.; Katzensteiner, A.; Bachmaier, A.; Mücklich, F.; Suárez, S. On the reinforcement homogenization in CNT/metal matrix composites during severe plastic deformation. *Mater. Charact.* **2018**, *136*, 375–381. [[CrossRef](#)]
23. Katzensteiner, A.; Aristizabal, K.; Suarez, S.; Pippan, R.; Bachmaier, A. Temperature dependent structural evolution in nickel/carbon nanotube composites processed by high-pressure torsion. In Proceedings of the IOP Conference Series: Materials Science and Engineering, Bristol, UK, 2017; Volume 194, No. 1, p. 01201.
24. Aristizabal, K.; Katzensteiner, A.; Leoni, M.; Mücklich, F.; Suárez, S. Evolution of the lattice defects and crystalline domain size in carbon nanotube metal matrix composites processed by severe plastic deformation. *Mater. Charact.* **2019**, *154*, 344–352. [[CrossRef](#)]
25. Katzensteiner, A.; Müller, T.; Kormout, K.; Aristizabal, K.; Suarez, S.; Pippan, R.; Bachmaier, A. Influence of Processing Parameters on the Mechanical Properties of HPT-Deformed Nickel/Carbon Nanotube Composites. *Adv. Eng. Mater.* **2019**, *21*, 1800422. [[CrossRef](#)]
26. Stüwe, H.P. Equivalent strains in severe plastic deformation. *Adv. Eng. Mater.* **2003**, *5*, 291–295. [[CrossRef](#)]
27. Reinert, L.; Zeiger, M.; Suárez, S.; Presser, V.; Mücklich, F. Dispersion analysis of carbon nanotubes, carbon onions, and nanodiamonds for their application as reinforcement phase in nickel metal matrix composites. *RSC Adv.* **2015**, *5*, 95149–95159. [[CrossRef](#)]
28. La, P.; Ma, J.; Zhu, Y.T.; Yang, J.; Liu, W.; Xue, Q.; Valiev, R.Z. Dry-sliding tribological properties of ultrafine-grained Ti prepared by severe plastic deformation. *Acta Mater.* **2005**, *53*, 5167–5173. [[CrossRef](#)]
29. Blau, P.J. On the nature of running-in. *Tribol. Int.* **2005**, *38*, 1007–1012. [[CrossRef](#)]
30. Blau, P.J. Running-in: Art or engineering? *J. Mater. Eng.* **1991**, *13*, 47–53. [[CrossRef](#)]
31. Wilson, S.; Alpas, A.T. Thermal effects on mild wear transitions in dry sliding of an aluminum. *Wear* **1999**, *225*, 440–449. [[CrossRef](#)]
32. Stachowiak, G. *Wear—Materials, Mechanisms and Practice*, 1st ed.; John Wiley & Sons: Hoboken, NJ, USA, 2005.
33. Scharf, T.W.; Neira, A.; Hwang, J.Y.; Tiley, J.; Banerjee, R. Self-lubricating carbon nanotube reinforced nickel matrix composites. *J. Appl. Phys.* **2009**, *106*, 013508. [[CrossRef](#)]
34. Aristizabal, K.; Katzensteiner, A.; Bachmaier, A.; Mücklich, F.; Suarez, S. Study of the structural defects on carbon nanotubes in metal matrix composites processed by severe plastic deformation. *Carbon* **2017**, *125*, 156–161. [[CrossRef](#)]

